J Solid State Electrochem (2010) 14:937–943
DOI 10.1007/s10008-009-0884-4

ORIGINAL PAPER

Characterizations of white-light $ZnWO_4$ phosphor prepared by blending complementary phosphor

Su-Hua Yang · Fu-Shou Tsai · Jia-Xing Chen

Received: 2 March 2009 / Revised: 6 June 2009 / Accepted: 9 June 2009 / Published online: 27 June 2009

Abstract In the preparation of $ZnWO_4$ phosphor, crystalline $ZnWO_4$ was created, even though the concentration of WO_3 was only 10 mol%. $ZnWO_4$ was the dominant crystallization phase when the concentration of WO_3 exceeded 40 mol%. The optimal crystallization of $ZnWO_4$ phosphor was obtained when the composition molar ratio of ZnO to WO_3 was 1:1, and sintering was carried out at 1,100°C for 3 h. In this condition, a bluish-green emission with a peak at 460 nm was observed. For Y_2O_3:Eu^{3+},Li^+, the complementary phosphor of $ZnWO_4$, the Li flux improved phosphor crystallization. The red emission peak of the Y_2O_3:Eu^{3+},Li^+ phosphor was measured at about 612 nm. The optimal photoluminescence intensity of the Y_2O_3:Eu^{3+},Li^+ phosphor was obtained when it was sintered at 1,200°C for 5 h and was mixed with 11 mol% Eu_2O_3 and 70 mol% Li_2CO_3. When the weight ratio of Y_2O_3:Eu^{3+},Li^+ to $ZnWO_4$ was 1:4, the Y_2O_3:Eu^{3+},Li^+-blended $ZnWO_4$ phosphor showed white-light emission with Commission Internationale de l'Eclairage coordinates at (0.34, 0.30). The luminance of the white-light phosphor excited by a 6-W UV lamp was around 160 cd/m^2.

Keywords Phosphor · Powder · Blend · Sintering · Photoluminescence

Introduction

Phosphor is a luminescent substance that emits light from one of the host ions by self-activated luminescence or from a dopant, called an activator, by direct or indirect excitation [1, 2].

To increase the luminescence efficiency of phosphor, researchers have tried various approaches. These include using different synthesis methods to modify phosphor particle size and surface morphology, adding conductive materials to increase the conductivity [3, 4], mixing flux materials to increase the extent of crystallization [5], and doping a sensitizer to enhance excitation energy absorption and energy transfer to the activator [6]. By choosing a suitable synthesis method, we can achieve high efficiency along with the desired emission color of the phosphor.

To date, white-light phosphors have attracted significant attention due to their applications as backlights and light sources. To prepare stable white-light phosphors exhibiting high luminance, oxide-based materials are preferred [7–9] because they have unique physical and chemical properties, high stability, and satisfactory broadband emission in the visible light region. In this study, a bluish-green $ZnWO_4$ phosphor was synthesized. It has the advantages of a high average refractive index, high X-ray absorption coefficient, and high light yield [8]. To achieve white-light luminescence, a complementary phosphor, Y_2O_3:Eu^{3+},Li^+, was blended with the $ZnWO_4$ phosphor; this complementary phosphor emits red-colored light. The preparation and characteristics of the $ZnWO_4$ and Y_2O_3:Eu^{3+},Li^+ phosphors were investigated, along with the luminescence properties of the Y_2O_3:Eu^{3+},Li^+-blended $ZnWO_4$ phosphor.

Experiments

In this study, the solid-state sintering method was used to synthesize the phosphors. For the preparation of $ZnWO_4$ phosphor, ZnO powder (99.999%), used as the source

S.-H. Yang (✉) · F.-S. Tsai · J.-X. Chen
Department of Electronic Engineering,
National Kaohsiung University of Applied Sciences,
Kaohsiung, Taiwan, Republic of China
e-mail: shya@cc.kuas.edu.tw

material, was mixed with WO_3 (99.9%) at different concentrations (10–60 mol%). The mixed powders were blended with deionized water then milled for 24 h. Subsequently, the solution was dried in an oven and sintered at 700–1,200°C for 1–8 h. Finally, the synthesized powders were ground, and the $ZnWO_4$ phosphor was prepared.

The Y_2O_3:Eu^{3+},Li^+ phosphor was prepared by the same process as that used to prepare $ZnWO_4$. In this condition, Y_2O_3 (99.99%) was adopted as the source material, and Eu_2O_3 (99.99%) and Li_2CO_3 (99.99%) were selected as the red dopant and flux, respectively. The concentrations of Eu_2O_3 and Li_2CO_3 were varied over ranges of 0–15 and 0–80 mol%, respectively. The Y_2O_3:Eu^{3+},Li^+ phosphor was synthesized at 600–1,200°C over a period of 1–8 h.

The surface morphology of the phosphor was visualized using a Philips XL-40 field emission scanning electron microscope (SEM) system operated at 10 kV. The crystallization was analyzed using a SIEMENS D5000 X-ray diffraction (XRD) system with Cu Kα radiation (λ=0.1541 nm) and recorded in the range of 2θ=10–70°. For photoluminescence (PL) measurements, a phosphor film was prepared on an indium-tin-oxide glass substrate by screen-printing. A Hitachi F-7000 fluorescence spectrophotometer equipped with a 150-W xenon lamp and a monochrometer was used to evaluate the PL and PL excitation (PLE) spectra. The excitation wavelength (λ_{ex}) of PL and the monitoring wavelength (λ_{em}) of PLE were respectively set at 325 and 460 nm for the $ZnWO_4$ phosphor and at 254 and 612 nm for the Y_2O_3:Eu^{3+},Li^+ phosphor. The luminance and Commission Internationale de l'Eclairage (CIE) coordinates of the phosphor were measured using a Minolta Chroma Meter model CS-100A. A 6-W UV lamp (1,200 μW/cm^2, wavelength of 254 nm) was used as the excitation source for luminance measurements; this lamp provides only two emission wavelengths of 254 and 365 nm.

Results and discussion

Characterizations of $ZnWO_4$ phosphor

Figure 1 shows the XRD patterns of the $ZnWO_4$ phosphor. When WO_3 was not used, the synthesized phosphor was a hexagonal wurtzite ZnO with crystallization planes of (100), (002), (101), (102), (110), and (103). The XRD patterns of $ZnWO_4$ phosphor sintered at 700°C for 3 h and synthesized using 10, 30, 40, and 60 mol% WO_3 are shown in Fig. 1b–e, respectively; the hollow square and circle symbols represent the $ZnWO_4$ and WO_3 phases, respectively. A developed $ZnWO_4$ crystal structure was evident, even though only a low concentration of WO_3, 10 mol%,

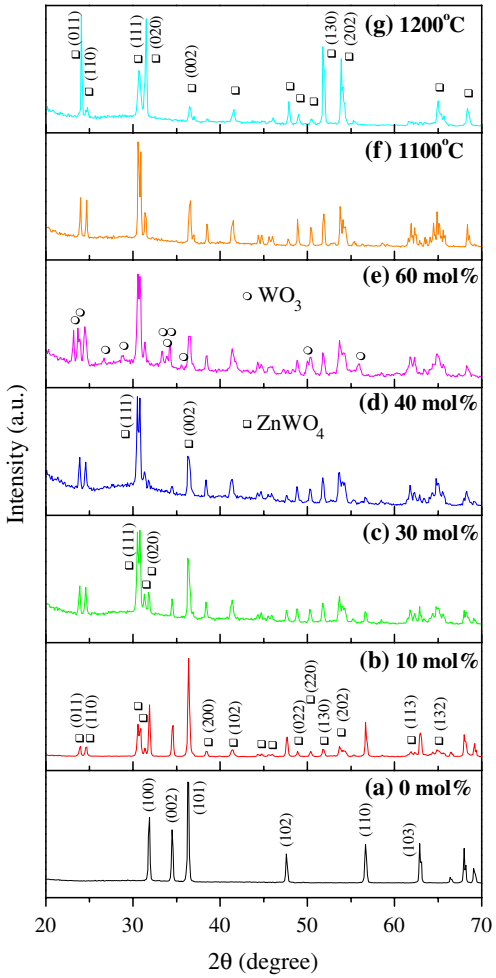

Fig. 1 X-ray diffraction patterns of the $ZnWO_4$ phosphor for different preparation conditions; WO_3 concentrations at (**a**) 0, (**b**) 10, (**c**) 30, (**d**) 40, and (**e**) 60 mol% and sintered at 700°C for 3 h; WO_3 concentration at 50 mol% and sintered at (**f**) 1,100°C and (**g**) 1,200°C for 3 h

was used during phosphor preparation. $ZnWO_4$ became the dominant crystalline phase, with a (111) main growth plane, when the concentration of WO_3 exceeded 40 mol%. However, an excess of WO_3 was observed when the WO_3 concentration was higher than 60 mol%. The atomic ratios of Zn to W were 6.90, 3.49, 1.20, 0.63, and 0.54% for phosphors sintered at 700°C and synthesized with 10, 30, 40, 50, and 60 mol% WO_3, respectively. Optimal crystallization was obtained in the case of the $ZnWO_4$ phosphor synthesized using 50 mol% WO_3 and sintered at 1,100°C for 3 h, as shown in Fig. 1f. In this condition, the atomic ratio of Zn to W was 0.68%. Figure 2a, b show the SEM images of $ZnWO_4$ synthesized at 700°C for 3 h using 10 and 50 mol% WO_3, respectively. When the phosphor was prepared at low temperatures, the grain size was almost unchanged even though the concentration of WO_3 was increased. The particle size of the phosphor shown in Fig. 2b was about 16.8 nm, evaluated from the XRD pattern

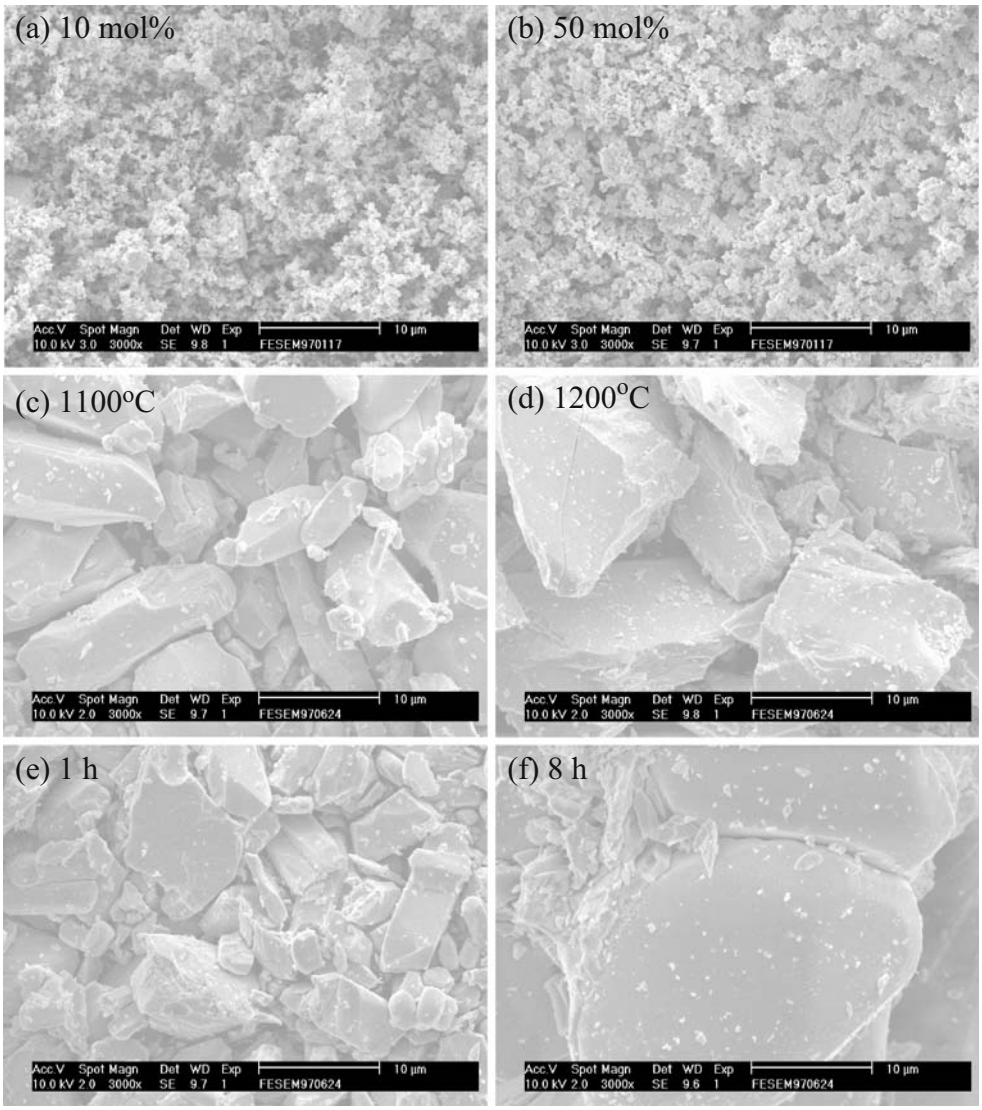

Fig. 2 Scanning electron microscope images of the $ZnWO_4$ phosphor prepared under different synthesis conditions; WO_3 concentrations at (**a**) 10 and (**b**) 50 mol% and sintered at 700°C for 3 h; WO_3 concentration at 50 wt% and sintered at (**c**) 1,100°C and (**d**) 1,200°C for 3 h; WO_3 concentration at 50 wt% and sintered at 1,100°C for (**e**) 1 and (**f**) 8 h

using the Scherrer equation [10]. For the phosphor prepared with 50 mol% WO_3, the full width at half maximum (FWHM) of the (111) $ZnWO_4$ peak obtained from the XRD patterns was 0.46, 0.39, 0.42, 0.42, and 0.31° for sintering temperatures of 800°C, 900°C, 1,000°C, 1,100°C, and 1,200°C, respectively. The crystallization of the $ZnWO_4$ phosphor was apparently improved by increasing the sintering temperature. Meanwhile, the decreased FWHMs in the XRD patterns show that the grain size of the phosphor increased with the sintering temperature. Improvement in crystallization normally accompanied an increase in phosphor particle size [11]. The particle sizes of $ZnWO_4$ phosphor were approximately 16.8, 17.9, 20.2, 19.6, 19.6, and 26.5 nm for sintering temperatures increasing in steps of 100°C from 700°C to 1,200°C, respectively. Figure 2b–d show SEM images of the $ZnWO_4$ phosphor synthesized using 50 mol% WO_3 at 700°C, 1,100°C, and 1,200°C for 3 h, respectively. It is evident that the phosphor grain size increases significantly with the sintering temperature; this result is consistent with the results of XRD analyses.

Furthermore, when the $ZnWO_4$ phosphor was prepared with 50 mol% WO_3 and synthesized at 1,200°C, the main growth plane of the phosphor changed from (111) to (011), and appreciable growths at (020), (130), and (202) planes were observed from the XRD analyses shown in Fig. 1g. It was also found that the main growth planes of the $ZnWO_4$ phosphor prepared at 50 mol% WO_3 and sintered at 1,100°C were altered from (111) to (020) and (130) when the sintering time was increased from 3 to 5 and 8 h, respectively. The change in the growth plane substantially modified the luminescence characteristics of the phosphor. Figure 2e, c, and f show SEM images of the $ZnWO_4$ phosphor synthesized using 50 mol% WO_3 and sintered at 1,100°C for 1, 3, and 8 h, respectively. Significant changes in grain shape and size were observed with an increase in

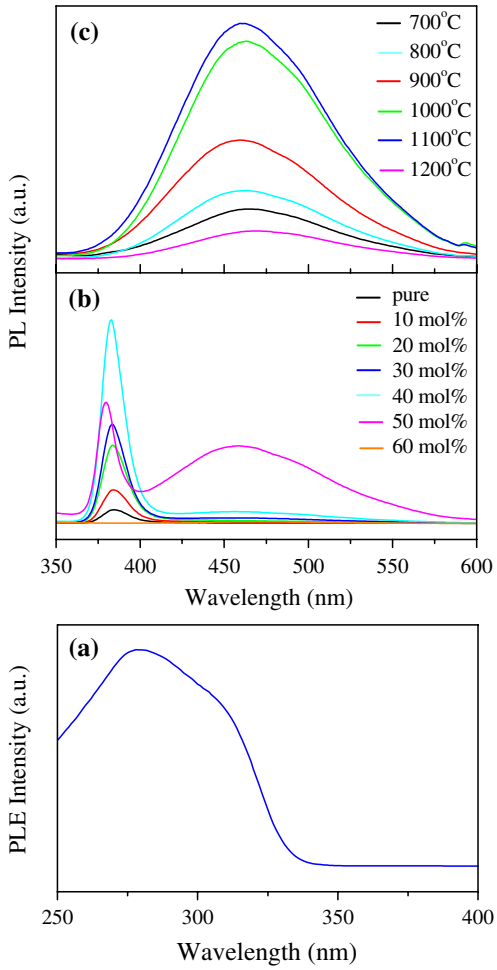

Fig. 3 Photoluminescence (PL) and PL excitation (PLE) characteristics of the $ZnWO_4$ phosphor. (**a**) PLE spectrum monitored at a wavelength of 460 nm. (**b**) PL spectra for different concentrations of WO_3 and sintered at 700°C for 3 h. (**c**) PL spectra for WO_3 concentration at 50 mol% and sintered at different temperatures for 3 h

the sintering time. Optimal crystallization was realized in the case of the $ZnWO_4$ phosphor synthesized using 50 mol% WO_3 at 1,100°C for 3 h. The maximum emission intensity was achieved when the phosphor exhibited optimal crystallization.

Figure 3a shows the PLE spectrum monitored at a wavelength of 460 nm for $ZnWO_4$ phosphor synthesized using 50 mol% WO_3 and sintered at 1,100°C for 3 h. The maximum absorption wavelength for the $ZnWO_4$ phosphor was 279 nm. In this study, the excitation wavelength of the $ZnWO_4$ phosphor was fixed at 325 nm for PL measurements. Figure 3b shows the PL spectra of the $ZnWO_4$ phosphor synthesized using different concentrations of WO_3 and sintered at 700°C for 3 h. Two emission bands in the UV and visible regions were observed. The UV band with a peak wavelength of approximate 384 nm was consistent with a near-band edge emission [12]. The blue-shift phenomenon in UV emission was observed when the WO_3 concentration was increased. This was due to the development of $ZnWO_4$ crystalline which has a bandgap 3.7 eV larger than the ZnO bandgap (3.2 eV) [13–15]. The maximum UV emission intensity was measured when the $ZnWO_4$ phosphor was synthesized using 40 mol% WO_3. However, when 50 mol% WO_3 was used, a visible bluish-green emission with a peak at 460 nm was observed. Obviously, $ZnWO_4$ shows a self-activated emission. The WO_6^{6-} octahedral structure in the $ZnWO_4$ matrix played the role of a luminescence center, in which the luminescence of W-O groups was due to charge transfers between the O 2*p* orbitals and the empty *d* orbitals of the central W^{6+} ion [8, 16–20]. If the WO_3 concentration was higher than 60 mol%, an excess of WO_3 was observed, and the concentration quenching effect then led to a decrease in PL intensity.

The PL spectra for $ZnWO_4$ phosphor synthesized using 50 mol% WO_3 and sintered at different temperatures for 3 h are shown in Fig. 3c. The PL intensity was enhanced when the sintering temperature was increased, which was attributed to an improvement in the crystallization of the phosphor [11]. The maximum PL intensity was obtained when the sintering temperature was 1,100°C. A significant decrease in PL intensity was measured when the phosphor was sintered at 1,200°C. This decrease was attributed to a change in the crystallization of the phosphor, in which (020) $ZnWO_4$ was the dominant crystalline. Empirically, the change in crystallinity alters the emission mechanisms of the phosphor. It was also found that the growth of larger phosphor grains (Fig. 2d) was another reason for the decrease in luminescence. Furthermore, Fig. 3c shows that the PL spectrum was broadened when the sintering temperature increased. Apparently, oxygen vacancies were involved in the phosphor crystal, and the bluish-green emission was related to electron transitions from the energy levels of the ionized oxygen vacancies to the phosphor valance band. The concentration of oxygen vacancies usually increases with an increase in sintering temperature [21], and a broadened emission is thus observed.

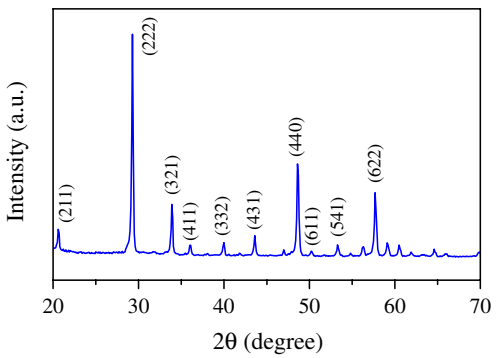

Fig. 4 Representative X-ray diffraction pattern of $Y_2O_3:Eu^{3+},Li^+$ phosphor

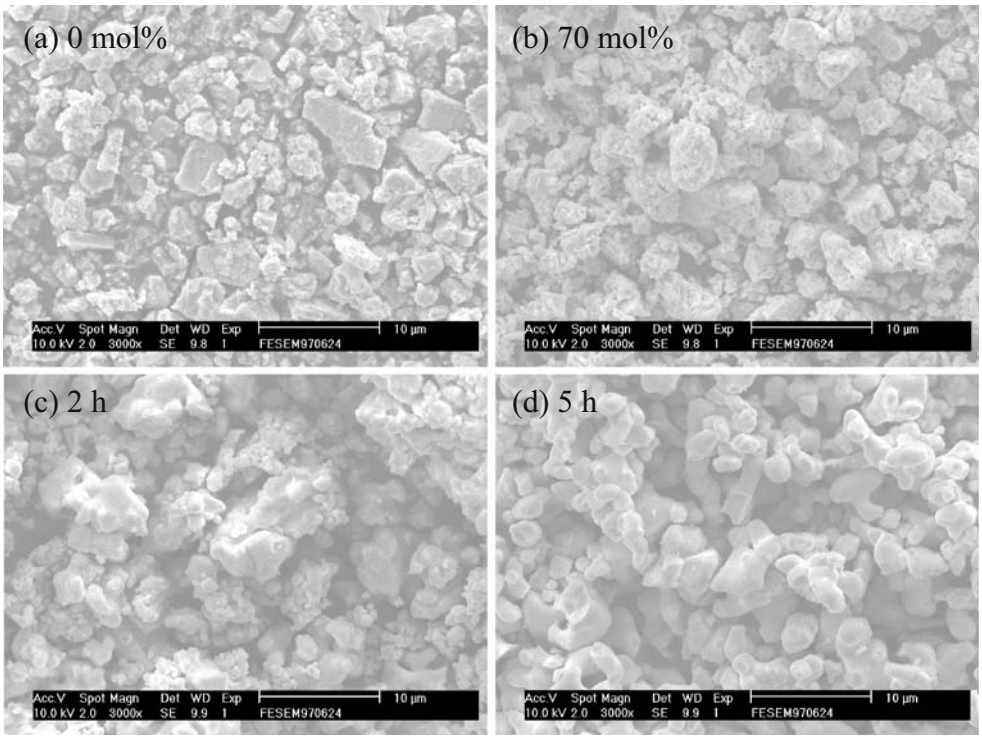

Fig. 5 Scanning electron microscope images of the 11 mol% Eu_2O_3 doped Y_2O_3:Eu^{3+},Li^+ phosphor prepared under different conditions; (**a**) without and (**b**) with 70 mol% Li_2CO_3 mixing and sintered at 800°C for 2 h; with 70 mol% Li_2CO_3 mixing and sintered at 1,200°C for (**c**) 2 and (**d**) 5 h

Characterizations of Y_2O_3:Eu^{3+},Li^+ phosphor

The recorded XRD patterns showed that (222) was the main growth plane of the Y_2O_3:Eu^{3+},Li^+ phosphors, and similar patterns were obtained, even if the preparation conditions were varied. Figure 4 shows the representative XRD pattern for the Y_2O_3:Eu^{3+},Li^+ phosphor. It was found that the FWHM of the (222) Y_2O_3:Eu^{3+},Li^+ peak decreased from 0.25° to 0.20° when Li_2CO_3 concentration was increased from 0 to 80 mol%. This was attributed to the flux of Li enhancing the crystalline growth of the Y_2O_3:Eu^{3+}, Li^+ phosphor. Consequently, an improvement in phosphor crystallization was measured [22]. SEM analyses showed that the phosphor grain size increased slightly with an increase of Li doping concentration; the particle sizes

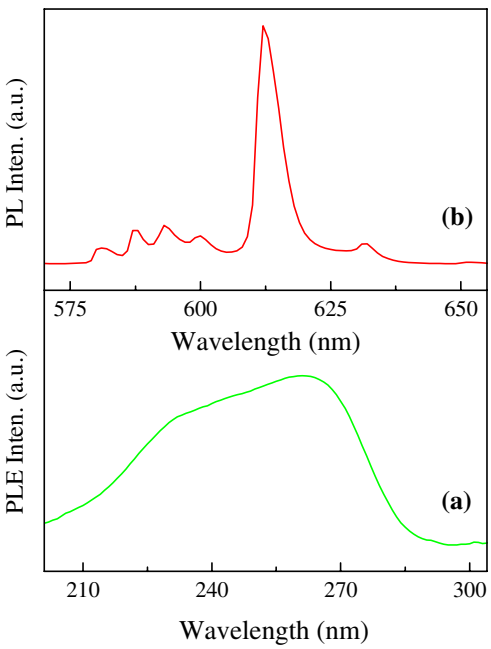

Fig. 6 (**a**) Photoluminescence excitation (PLE) spectrum monitored at a wavelength of 612 nm and (**b**) photoluminescence spectrum excited at a wavelength of 254 nm for the Y_2O_3:Eu^{3+},Li^+ phosphor

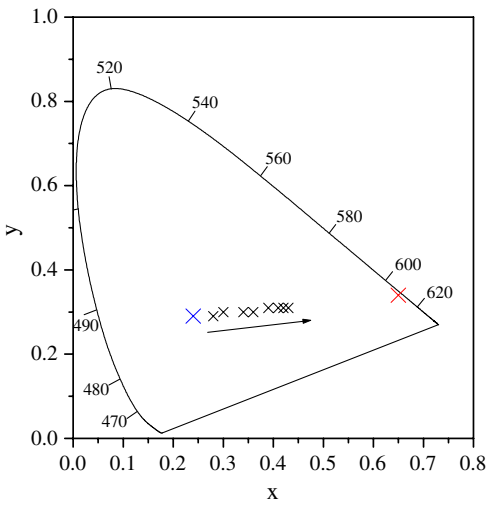

Fig. 7 Commission Internationale de l'Eclairage (CIE) coordinates of the Y_2O_3:Eu^{3+},Li^+-blended $ZnWO_4$ phosphor for different weight ratios of Y_2O_3:Eu^{3+},Li^+, where *blue*, *red*, and *black symbols* represent the CIE coordinates of the $ZnWO_4$, Y_2O_3:Eu^{3+},Li^+, and blended phosphor, respectively

Table 1 CIE coordinates and color temperature of the Y_2O_3:Eu,Li-blended $ZnWO_4$ phosphors for different weight ratios

Blend ratio of Y_2O_3:Eu,Li to $ZnWO_4$ (wt%)	CIE coordinates		Color temperature
	x	y	(K)
0:1	0.24	0.29	16,033
1:12	0.28	0.29	9,972
2:12	0.30	0.30	7,738
3:12	0.34	0.30	5,028
4:12	0.36	0.30	3,983
5:12	0.39	0.31	3,037
6:12	0.41	0.31	2,574
7:12	0.42	0.31	2,394
8:12	0.43	0.31	2,241
1:0	0.65	0.34	1,000

evaluated from XRD patterns were around 32.8–41.0 nm as the Li_2CO_3 concentrations were varied from 0–80 mol%. Moreover, for the phosphor doped with 11 mol% Eu_2O_3 and sintered at 800°C for 2 h, a flake-like grain shape was observed when the phosphor was prepared without Li_2CO_3 mixing (Fig. 5a). However, a rounded phosphor grain shape was observed with Li_2CO_3 mixing, as shown in Fig. 5b, where the Y_2O_3:Eu^{3+},Li^+ phosphor was synthesized using 70 mol% Li_2CO_3 and 11 mol% Eu_2O_3. Additionally, a small change in FWHM of the (222) Y_2O_3:Eu^{3+},Li^+ peak, 0.19–0.24°, was measured when the doping concentration of Eu_2O_3 was varied in the range 0–15 mol%. Slight changes in phosphor grain size were due to the ionic crystal radius of Eu^{3+} (0.095 nm) being close to that of Y^{3+} (0.090 nm). However, a high doping concentration of Eu_2O_3 caused a decay in the crystallization of the Y_2O_3:Eu^{3+},Li^+ phosphor. It was also found that the crystallization of Y_2O_3:Eu^{3+},Li^+ was improved by increasing the sintering temperature (600–1,200°C) and sintering time (1–8 h). Figure 5c and d show the SEM images for Y_2O_3:Eu^{3+},Li^+ phosphor synthesized using 11 mol% Eu_2O_3 and 70 mol% Li_2CO_3 and sintered at 1,200°C for 2 and 5 h, respectively. Based on Fig. 5, it revealed that the growth of phosphor particles became more obvious when the sintering temperature and time were increased.

Figure 6a shows the PLE spectrum monitored at λ_{em}= 612 nm for the Y_2O_3:Eu^{3+},Li^+ phosphor synthesized using 11 mol% Eu_2O_3 and 70 mol% Li_2CO_3 and sintered at 1,200°C for 5 h. A broadband PLE spectrum with a peak at 261 nm was observed, which was related to the electron transfer from neighboring oxygen anions' 2*p* state to the Eu^{3+} ions' 4*f* state [23]. The PL spectrum of the Y_2O_3:Eu^{3+}, Li^+ phosphor for the excitation wavelength at 254 nm is shown in Fig. 6b. This emission is related to the electron transfer from the excited $5D_o$ state to the ^7F_J levels of the Eu^{3+} ions, where J=0, 1, and 2. The weak emissions at wavelengths of 578–590 nm are due to $5D_o \rightarrow {}^7F_0$ forbidden electric dipole transition, and those in the vicinity of 590–605 nm are attributed to $5D_o \rightarrow {}^7F_1$ magnetic dipole transition. The emission band at around 605–637 nm with a peak at about 612 nm is due to $5D_o \rightarrow {}^7F_2$ hypersensitive electric dipole transition, which is caused by the lack of inversion symmetry at the Eu^{3+} sites [9, 20, 24, 25]. The PL intensity initially increased as the Eu doping concentration increased, and a concentration quenching effect was observed at higher Eu doping concentrations. The variation in PL intensity correlated with the Li_2CO_3 mixing concentration was similar to that associated with the Eu_2O_3 doping concentration. An increase in PL intensity by a factor of 72 was measured when the phosphor was mixed with Li_2CO_3. This was attributed to an improvement in crystallinity, which led to higher oscillating strengths for optical transitions [26]. Furthermore, the PL intensity was enhanced due to the improved crystallinity of the Y_2O_3:Eu^{3+}, Li^+ phosphor by increasing both the sintering temperature and time. Nevertheless, Y_2O_3:Eu^{3+},Li^+ phosphor synthesized for 8 h led to a decay in PL intensity because of the growth of larger phosphor grains; a similar phenomenon was observed in the $ZnWO_4$ phosphor. The optimal red PL was achieved when the Y_2O_3:Eu^{3+},Li^+ phosphor was

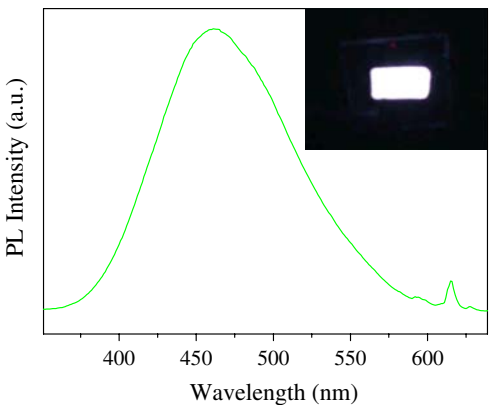

Fig. 8 Photoluminescence spectrum and emission image (inset) of the white-light Y_2O_3:Eu^{3+},Li^+-blended $ZnWO_4$ phosphor

synthesized using 11 mol% Eu_2O_3 and 70 mol% Li_2CO_3 and sintered at 1,200°C for 5 h.

Characterizations of white-light phosphor

PL measurements confirmed that the emission peaks for the $ZnWO_4$ and Y_2O_3:Eu^{3+},Li^+ phosphors were at 460 and 612 nm, respectively. The CIE coordinates were at (0.24, 0.29) for $ZnWO_4$ and (0.65, 0.34) for Y_2O_3:Eu^{3+},Li^+ when phosphors were prepared at optimal PL intensity. Significantly, white-light phosphor could be achieved if the bluish-green $ZnWO_4$ and red Y_2O_3:Eu^{3+},Li^+ phosphors were blended.

Figure 7 shows the CIE coordinates of the Y_2O_3:Eu^{3+}, Li^+-blended $ZnWO_4$ phosphors for different blending weight ratios, where both the Y_2O_3:Eu^{3+},Li^+ and the $ZnWO_4$ phosphors were prepared under optimal conditions. The blue, red, and black symbols represent the CIE coordinates of the $ZnWO_4$, Y_2O_3:Eu^{3+},Li^+, and blended phosphors, respectively. In this figure, the CIE coordinates exhibit a linear red shift phenomenon with the increasing weight ratio of the red Y_2O_3:Eu^{3+},Li^+ phosphor. Table 1 listed the variations in CIE coordinates and color temperature with the changes in the weight ratio of Y_2O_3:Eu^{3+},Li^+ to $ZnWO_4$. When the weight ratio of Y_2O_3:Eu^{3+},Li^+ to $ZnWO_4$ was 1:4, the blended phosphor showed a white-light emission, with CIE coordinates at (0.34, 0.30). The PL spectrum of the white-light Y_2O_3:Eu^{3+},Li^+-blended $ZnWO_4$ phosphor is shown in Fig. 8. The luminance was around 160 cd/m^2 when it was excited by a 6-W UV lamp (1,200 μW/cm^2, wavelength at 254 nm). The emission image of the white-light Y_2O_3:Eu^{3+},Li^+-blended $ZnWO_4$ phosphor is shown in the inset of Fig. 8.

Conclusions

XRD analyses showed that (101) was the main growth plane of the $ZnWO_4$ phosphor. When the concentration of WO_3 was above 40 mol%, the $ZnWO_4$ was the dominant phase, with a (111) main growth plane. When the $ZnWO_4$ phosphor was synthesized at a higher temperature of 1,200°C, the main growth plane changed to (011). The changes in the growth plane and crystallization substantially modified the luminescence characteristics of the phosphor. When the concentration of WO_3 was 50 mol%, a bluish-green emission with a peak at 460 nm of the $ZnWO_4$ phosphor was recorded. A broadened PL spectrum was measured when the sintering temperature was increased due to the increased oxygen vacancy concentration. In addition, the Y_2O_3:Eu^{3+}, Li^+ phosphor showed an improvement in crystallization and an increase in phosphor particle size by Li_2CO_3 mixing. The flake-like and rounded grain shapes of the Y_2O_3:Eu^{3+},Li^+ phosphor were seen when the phosphor was synthesized without and with Li_2CO_3 mixing, respectively. Meanwhile, when the doping concentration of Eu_2O_3 varied, a slight change in phosphor grain size was observed. The PL peak of the Y_2O_3:Eu^{3+},Li^+ phosphor was 612 nm. It was found that the Y_2O_3:Eu^{3+},Li^+-blended $ZnWO_4$ phosphor exhibited a white-light emission. When the weight ratio of Y_2O_3:Eu^{3+}, Li^+ to $ZnWO_4$ was 1:4, the CIE coordinates of the blended phosphor were at (0.34, 0.30).

Acknowledgement The authors thank the National Science Council of the Republic of China for financially supporting this work under contract No. NSC 97-2221-E-151-05.

References

1. Wu SH, Cheng HC (2004) J Electrochem Soc 151:H159
2. Park JK, Kim JM, Oh ES, Kim CH (2005) Electrochem Solid-State Lett 8:H6
3. Kominami H, Nakamura T, Sowa K, Nakanishi Y, Hatanaka Y, Shimaoka G (1997) Appl Surf Sci 113/114:519
4. Kim GC, Kim JS, Oh ES, Choi JC, Jeong K, Chang SK, Park HL, Kim TW, Kim CD (2000) Mater Res Bull 35:2409
5. Shin SH, You YC, Lee SH (2004) J Electrochem Soc 151:H40
6. Jia D (2006) J Electrochem Soc 153:H198
7. Hao J, Cocivera M (2001) Appl Phys Lett 79:740
8. Lou Z, Hao J, Cocivera M (2002) J Lumin 99:349
9. Hao J, Lou Z, Renaud I, Cocivera M (2004) Thin Solid Films 467:182
10. Bansal NP, Zhong Z (2006) J Power Sources 158:148
11. Kang YC, Lenggoro IW, Park SB, Okuyama K (1999) J Solid State Chem 146:168
12. Hong R, Shao J, He H, Fan Z (2005) J Cryst Growth 284:347
13. Bonanni M, Spanhel L, Lerch M, Füglein E, Müller G (1998) Chem Mater 10:304
14. Yi L, Hou Y, Zhao H, He D, Xu Z, Wang Y, Xu X (2000) Displays 21:147
15. Li YY, Li YX, Wu YL, Sun WL (2007) J Lumin 126:177
16. Bonanni M, Spanhel L, Lerch M, Füglein E, Müller G (1998) Chem Mater 10:304
17. Huang J, Gao L (2006) J Am Ceram Soc 89:3877
18. Wang ZL, Li HL, Hao JH (2008) J Electrochem Soc 155:J152
19. Dafinova R, Papazova K, Bojinova A (1997) J Lumin 75:51
20. Wang H, Lin CK, Liu XM, Lin J, Yu M (2005) Appl Phys Lett 87:181907
21. Vanheusden K, Seager CH, Warren WL, Tallant DR, Voigt JA (1996) Appl Phys Lett 68:403
22. Cho JY, Do YR, Huh YD (2006) Appl Phys Lett 89:131915
23. Pang Q, Shi J, Liu Y, Xing D, Gong M, Xu N (2003) Mater Sci Eng B103:57
24. Murugan AV, Viswanath AK, Ravi V, Kakade BA, Saaminathan V (2006) Appl Phys Lett 89:123120
25. Annapurna K, Dwivedi RN, Buddhudu S (2002) Mater Lett 53:359
26. Yi SS, Bae JS, Moon BK, Jeong JH, Park JC, Kim IW (2002) Appl Phys Lett 81:3344